



Effects of Ni doping contents on photocatalytic activity of B–BiVO₄ synthesized through sol–gel and impregnation two-step method

Min WANG, Guang-jun YANG, Mei-yan YOU, Yuan-hua XIE, You-zhao WANG, Jin HAN, Tong ZHU

School of Mechanical Engineering and Automation, Northeastern University, Shenyang 110165, China

Received 29 May 2016; accepted 26 September 2016

Abstract: To enhance the photocatalytic activity of B–BiVO₄, Ni-doped B–BiVO₄ photocatalyst (Ni–B–BiVO₄) was synthesized through sol–gel and impregnation method. The photocatalysts were characterized by XPS, XRD, SEM, EDS, BET and UV–Vis DRS techniques. The results showed that single or double doping did not change the crystalline structure and morphology, but the particle size decreased with Ni doping. The band gap energy absorption edge of Ni–B–BiVO₄ shifted to a longer wavelength compared with undoped, B or Ni single doped BiVO₄. More V⁴⁺ and surface hydroxyl oxygen were observed in BiVO₄ after Ni–B co-doping. When the optimal mass fraction of Ni is 0.30%, the degradation rate of MO in 50 min is 95% for 0.3Ni–B–BiVO₄ sample which also can effectively degrade methyl blue (MB), acid orange (AOII) II and rhodamine B (RhB). The enhanced photocatalytic activity is attributed to the synergistic effects of B and Ni doping.

Key words: co-doping; Ni doping; BiVO₄; photocatalyst; sol–gel method; impregnation method

1 Introduction

In past decades, bismuth vanadate (BiVO₄) has attracted considerable attention for its visible light-driven photocatalytic activity in water splitting and organic pollutant degradation [1–3]. However, the poor photocatalytic efficiency of pure BiVO₄, which is due to its low quanta yield ratio, is one of the restrictions for its widespread application in the wastewater treatment [4–6].

Therefore, the challenge to overcome the above drawbacks remains. Metal doping has proven to be an effective approach to enhance the photocatalytic activity of BiVO₄ [7–15]. ZHANG et al [8] reported that Ag, Co and Ni doping of BiVO₄ can effectively enhance the photocatalytic activity for the degradation of methyl blue and 2,4-dichlorophenol. CHEN et al [9] prepared the Ni–BiVO₄ photocatalysts with a hydrothermal method. Compared with pure BiVO₄, the Ni–BiVO₄ catalyst shows a red shift in the absorption band in the visible region and a narrow band gap (2.35 eV). The Ni doping enhanced photocatalytic activities for the degradation of

methylene blue (MB) under visible light irradiation. ZHANG et al [10] prepared a CuO–BiVO₄ hetero-junction composite, which exhibited an enhanced photocatalytic activity for methylene blue (MB) degradation under visible light irradiation. It was found that the 5%CuO-loaded (mass fraction) composite can apparently enhance the photocatalytic activity for MB dye. Additionally, it was reported that F [16], S [17], N [18,19] and B [20–22] can also effectively enhance the photocatalytic activity of BiVO₄. JIANG et al [16] prepared F-doped BiVO₄ with a hydrothermal method using NH₄F as the fluoride source. It has been shown that F can effectively enhance the photodegradation rate of phenol. ZHAO et al [17] reported the sulfur doping of BiVO₄ prepared through a dodecylamine-assisted alcohol-hydrothermal route with Na₂S as sulfur source. Our team prepared N- [18] and B- [20,21] doped BiVO₄ by sol–gel method, a catalyst that can also effectively enhance the photocatalytic degradation of methyl orange under visible light irradiation.

In recent years, photocatalysts co-doped with metals and nonmetals have attracted more and more attention due to their enhanced photocatalytic activity [23–27].

Foundation item: Projects (21207093, 51004072) supported by the National Natural Science Foundation of China for Youth; Project (LJQ2014023) supported by the Liaoning Excellent Talents in University, China; Project (L20150178) supported by the General Scientific Research Projects Foundation of Liaoning Educational Committee, China; Project (N140303002) supported by the Fundamental Research Funds for the Central Universities, China

Corresponding author: Tong ZHU; Tel: +86-13940281581; E-mail: tongzhu@mail.neu.edu.cn
DOI: 10.1016/S1003-6326(17)60227-9

For example, PATEL et al [24] prepared TiO₂, N-doped TiO₂, V-doped TiO₂, and V–N-co-doped TiO₂ thin films. It was observed that the co-doped TiO₂ showed the best photocatalytic performance compared with the mono-doped and pure TiO₂ because of higher visible light absorption and possible decrease in recombination of photo-generated charges. KIMA et al [25] synthesized Fe–N-co-doped TiO₂ photocatalyst with a sonochemical method. The photocatalytic activity of Fe–N-co-doped TiO₂ for the degradation of indigo carmine dye (ICD) under solar simulator was enhanced when compared with TiO₂-P25 and N–TiO₂. WANG et al [26,27] prepared B and rare earth ions (Eu and La) co-doped BiVO₄ via a one-step sol–gel method. It shows that the synergetic effects between two co-doping elements can effectively enhance the photocatalytic activity of BiVO₄ under visible light irradiation.

Different preparation methods may result in different effects. Therefore, in the present work, we used sol–gel and impregnation two-step method to prepare B and Ni co-doped BiVO₄ photocatalysts to further enhance the photocatalytic activity for the degradation of methyl orange (MO), methyl blue (MB), acid orange II (AOII), and rhodamine B (RhB). The serials *x*Ni–B–BiVO₄ samples prepared by this method were characterized by XPS, XRD, SEM, BET and DRS techniques. The effects of the doping nickel amount on the properties of B-doped BiVO₄ were also investigated, and the synergetic effects between boron and nickel were studied.

2 Experimental

2.1 Photocatalyst preparation

In this experiment, we prepared the Ni–B co-doped BiVO₄ in two steps as follows.

Step 1: The B–BiVO₄ and pure BiVO₄ precursors were prepared through sol–gel method according to Ref. [21].

Step 2: 3 g B-doped BiVO₄ precursor was impregnated at 80 °C with an aqueous solution of Ni(NO₃)₂·6H₂O until the solution was dry. The resulting powder was collected and calcined in air in a muffle furnace at 500 °C for 5 h, and then cooled to room temperature to obtain *x*Ni–B–BiVO₄ nanoparticles. The Ni doping content (*x*) was chosen as 0.20%, 0.25%, 0.30%, 0.35% and 0.40%, respectively, which is the mass fraction of Ni(NO₃)₂·6H₂O to BiVO₄. Ni-doped BiVO₄ was prepared with the same impregnation method and its precursor is pure BiVO₄. Pure BiVO₄ and B–BiVO₄ were prepared in the same way as references for direct comparison [21].

2.2 Characterization and measurements

The crystal phases of the samples were investigated

by X-ray diffraction (XRD) with Cu K_α radiation (model D/max RA, Rigaku, Japan). The accelerating voltage and the applied current were 40 kV and 150 mA, respectively. The morphology of the samples was checked by a scanning electron microscope (SEM, S–3000N, Hitachi, Japan), coupled to an energy-dispersive X-ray spectrometer (EDX, Oxford Instrument). The binding energies of Bi, V, Ni, B and O were measured at room temperature using an X-ray photoelectron spectroscopy (XPS, VGESCALAB MARK II) using Mg K_α radiation. The Brunauer–Emmett–Teller (BET) surface area of the sample was obtained from nitrogen adsorption–desorption isotherms determined at liquid nitrogen temperature on an automatic analyzer (Autosorb-iQ-MP, Quantachrome, USA). The diffuse reflectance spectra (DRS) were investigated by a UV–Vis spectrophotometer (TU–1901, Puxi, China) equipped with an integrating sphere assembly using BaSO₄ as the reflectance standard. The spectra were recorded in the wavelength range of 230 to 800 nm at (25±1) °C.

2.3 Photocatalytic activity tests

The photocatalytic activities of the as-synthesized samples were measured by the photodegradation of MO, AOII and RhB solutions. A 250 W halogen lamp equipped with a cutoff filter smaller than 420 nm was used as the visible light source and was placed at approximately 14 cm from the reactor. The photodegradation experiment was performed as follows: 0.01 g of catalyst was added into a 50 mL solution of 15 mg/L MO (the concentrations of MB, AOII and RhB are 10, 15 and 15 mg/L, respectively). Prior to irradiation, the suspension was stirred in the dark for 60 min until the adsorption/desorption equilibrium was established. At given time intervals, the collected samples were filtered through a 0.45 μm millipore filter to remove the catalyst particles. The filtrate concentration was monitored by recording the absorbance at 464 nm using a UV–1800 UV–Vis spectrophotometer (Puxi, China).

3 Results and discussion

3.1 XPS analysis

The analysis of XPS spectra was performed to investigate the chemical states and chemical compositions of the samples. The Ni 2p high-resolution XPS scan spectrum is shown in Fig. 1(a). From Fig. 1(a), the Ni 2p spectrum of 0.3Ni–B–BiVO₄ consists of two strong symmetrical peaks at *E*_b=856.4 and 861.2 eV, corresponding to the Ni 2p_{3/2} and Ni 2p_{1/2} signals, which are characteristic of the Ni²⁺ species [9].

The B 1s XPS spectra of the B-doped and Ni–B-co-doped samples are shown in Figs. 1(b) and (c). Each XPS spectrum of B 1s exhibits an asymmetric broad

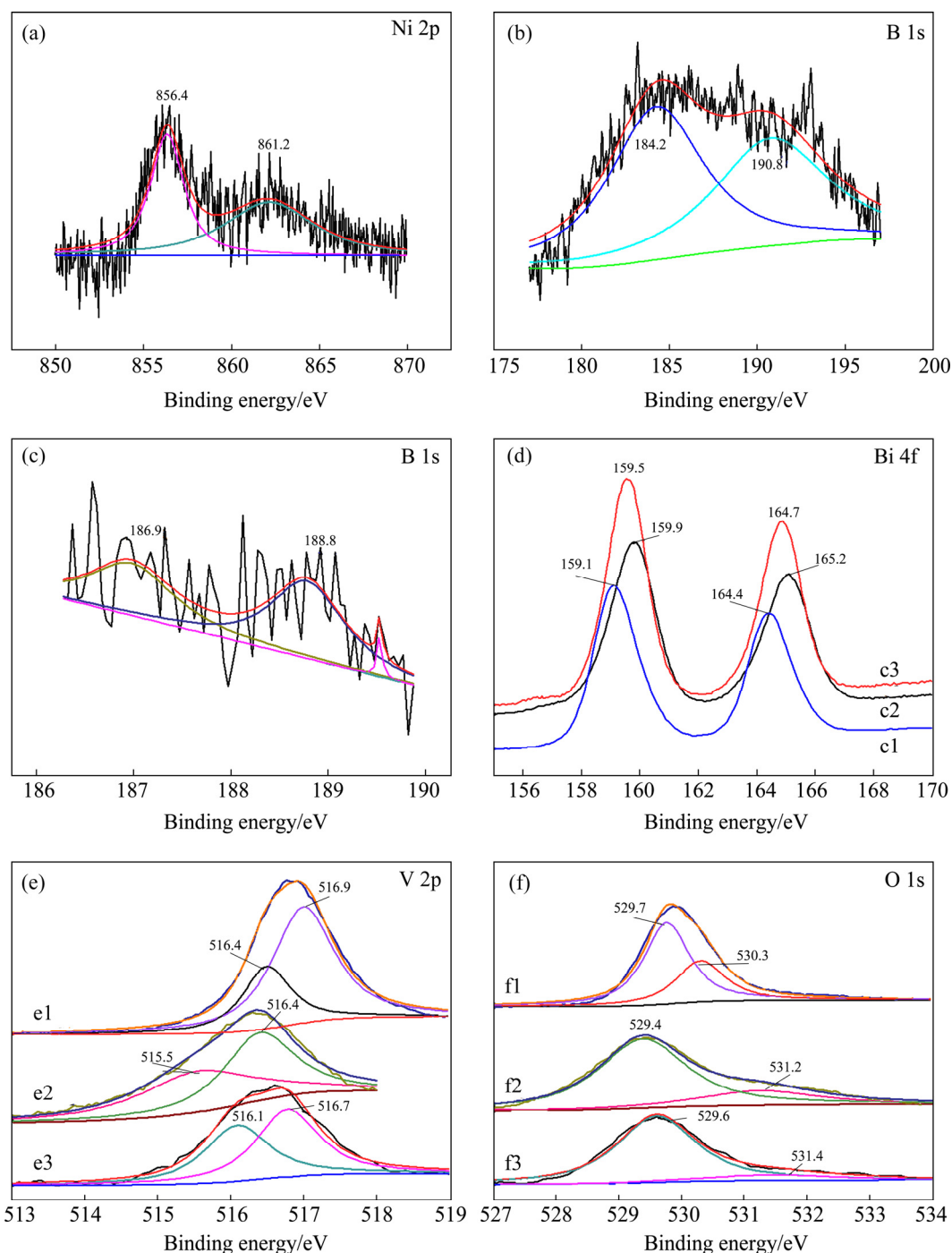


Fig. 1 Ni 2p (a), B 1s (b, c), Bi 4f (d), V 2p (e) and O 1s (f) XPS spectra of BiVO₄ (1), B-BiVO₄ (2) and 0.3Ni-B-BiVO₄ (3)

peak from 184 to 191 eV, which is a typical characteristic peak for B 1s species. The asymmetric peak is decomposed into two components at $E_b=184.2$ and 190.8 eV for B-BiVO₄, and $E_b=186.9$ and 188.8 eV for 0.3Ni-B-BiVO₄. The peaks at $E_b=184.2$ and 186.9 eV are assigned to B₄C [20] which shows no photocatalytic activity. The standard binding energies for B 1s in B₂O₃, H₃BO₃ (B—O bond), and VB₂ (V—B bond) are 193.6 [28], 193.0 [29] and 188.3 eV [21], respectively. There is no doubt that the B atoms are not

bonded by means of B—V—B bond or B—O bond. It may be concluded that some of the B atoms might be doped in the BiVO₄ lattice and replaced the O atoms to form a B—Bi—O bond [20].

After further doping with Ni, the binding energy of B 1s changes to 188.8 eV, which is comparable to the standard binding energy for B 1s in NiB (188.9 eV), probably because the doping Ni²⁺ ions replace some Bi³⁺ ions to form B—Ni—O bonds [9]. However, the binding energy of Ni in the 0.3Ni-B-BiVO₄ sample is 856.4 eV,

which is higher than that of Ni in NiB (852.4–854.2 eV). We can therefore deduce that no NiB phase appears in BiVO_4 (as shown in Fig. 1(a)). Moreover, the electron density of B increases due to the lower electronegativity of Ni compared with that of Bi, while the binding energy of B 1s decreased. The XPS results show that both boron and nickel are successfully doped into the BiVO_4 lattice.

Figure 1(d) shows the Bi 4f high-resolution XPS scan spectra of pure BiVO_4 , B- BiVO_4 , and 0.3Ni-B- BiVO_4 . The binding energies of Bi 4f appear at 159.1–159.5 eV and 164.4–165.2 eV for Bi 4f_{7/2} and Bi 4f_{5/2}, respectively, which are characteristics of the Bi³⁺ species [12,17]. However, the binding energies are different: $E_b=159.1$ and 164.4 eV for BiVO_4 , $E_b=159.9$ and 165.2 eV for B- BiVO_4 , $E_b=159.5$ and 164.7 eV for 0.3Ni-B- BiVO_4 . Compared with undoped BiVO_4 (159.1 and 164.4 eV for Bi 4f_{7/2} and Bi 4f_{5/2}, respectively), the Bi 4f peaks of B-doped (159.9 and 165.2 eV), and Ni-B co-doped samples (159.5 and 164.7) slightly shift by 0.8 and 0.4 eV, respectively, towards higher binding energy. The results indicate that B or/and Ni have been incorporated in the BiVO_4 crystal lattice, and the electron density of Bi consequently decreases because of the lower electronegativity of B with respect to O and the lower electronegativity of Ni with respect to Bi.

The V 2p XPS spectra of pure BiVO_4 , B- BiVO_4 and 0.3Ni-B- BiVO_4 are shown in Fig. 1(e). The asymmetric V 2p_{3/2} signals are decomposed into two peaks at 1) $E_b=516.1$ and 516.7 eV for BiVO_4 , 2) $E_b=515.5$ and 516.4 eV for B- BiVO_4 , and 3) $E_b=515.7$ and 516.3 eV for 0.3Ni-B- BiVO_4 and are attributed to the surface V⁴⁺ and V⁵⁺ species, respectively [20]. The surface V⁴⁺/V⁵⁺ molar ratio is 0.85 for BiVO_4 , 0.98 for B- BiVO_4 and 1.24 for 0.3Ni-B- BiVO_4 . The molar ratio increases with B and Ni doping into the crystal lattice of BiVO_4 . According to the electro-neutrality principle, one can deduce that the BiVO_4 samples are oxygen-deficient, and the amount of nonstoichiometric oxygen is dependent on the surface V⁴⁺/V⁵⁺ molar ratios.

As shown in Fig. 1(f), XPS spectrum of each O 1s shows a broad asymmetric peak, which can be fitted into two peaks. One stronger peak at ~530.07 eV corresponds to the bulk oxygen bonded to V or Bi [16]. The other peak at 530–531 eV is attributed to the surface hydroxyl oxygen [16]. The molar ratios of O_{ads}/O_{latt} in the undoped, B-doped, and B-Ni co-doped samples evaluated by the XPS analysis are 0.14, 0.85 and 1.59, respectively. Obviously, the B and Ni co-doping further increases the surface hydroxyl.

3.2 XRD and SEM analysis

To investigate the crystalline forms and crystallinities of the pure and doped samples, the XRD

patterns of the as-prepared samples are presented in Fig. 2. These peaks are attributed to monoclinic BiVO_4 (JCPDS cards No. 75–1866), as indexed in Fig. 2. No other phases can be found. However, the diffraction peaks observed for the doped samples are sharper than those of pure BiVO_4 , which indicates an increase of the crystallinity. Through using the Debye–Scherrer equation, the crystallite sizes of all the samples, calculated for the (121) peak, are shown in Table 1. It shows that the crystallite sizes decrease when the amount of Ni doping increases. Because the ionic radius of Ni²⁺ (0.0690 nm) is smaller than that of Bi³⁺ (0.1110 nm), the Ni²⁺ ion might replace Bi³⁺ ion in B- BiVO_4 , as verified by the XPS results.

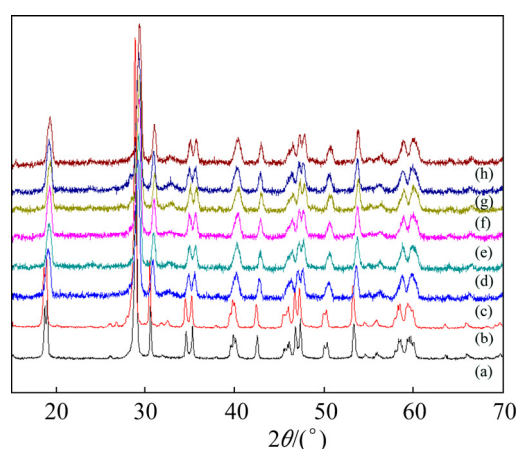


Fig. 2 XRD patterns of BiVO_4 (a), B- BiVO_4 (b), 0.30Ni- BiVO_4 (c), 0.20Ni-B- BiVO_4 (d), 0.25Ni-B- BiVO_4 (e), 0.30Ni-B- BiVO_4 (f), 0.35Ni-B- BiVO_4 (g) and 0.40Ni-B- BiVO_4 (h)

Table 1 Some selected properties of samples

Sample	D/nm	MO initial adsorption amount/%	Specific surface area/ $(\text{m}^2 \cdot \text{g}^{-1})$	Band gap/eV
BiVO_4	49.20	3.2	2.09	2.40
B- BiVO_4	47.61	6.6	2.41	2.36
0.30Ni- BiVO_4	48.62	5.2	2.96	2.38
0.20Ni-B- BiVO_4	47.15	6.2	2.78	2.33
0.25Ni-B- BiVO_4	47.02	6.9	2.95	2.30
0.30Ni-B- BiVO_4	46.52	7.2	3.05	2.26
0.35Ni-B- BiVO_4	46.21	7.0	3.56	2.24
0.40Ni-B- BiVO_4	46.10	7.0	3.49	2.22

The surface morphologies and particle sizes of pure BiVO_4 , B- BiVO_4 , and Ni-B- BiVO_4 were observed by SEM (Fig. 3). The BiVO_4 samples display a sphere-like morphology, and the particles are uniform in size. There is little difference in the morphologies between pure BiVO_4 and B- BiVO_4 . But, the size of some particles

decreases after Ni doping, indicating that Ni-doping can inhibit particle growth. The composition of the 0.30Ni–B–BiVO₄ sample was determined by energy dispersive X-ray spectroscopy (EDX). As shown in Fig. 3(d), the signals for Bi, V, O and Ni are quite obvious.

The BET specific surface areas of the as-prepared samples were measured using a nitrogen adsorption BET method (shown in Table 1). Ni–B co-doping can slightly enhance the specific areas of samples.

3.3 UV–Vis diffuse reflectance spectra

Figure 4 shows the UV–Vis diffuse reflectance spectra (DRS) of the Ni–B co-doped BiVO₄ samples

compared with pure, B-doped and Ni-doped BiVO₄. Due to the introduction of B dopants, a red shift of the absorption spectrum occurred. WANG et al [21] proposed that the visible light response was due to the narrowing of the band gap induced by mixing B 1s and O 2p states. The d-electrons of the doping Ni ions transfer to the conducting band of BiVO₄ [8], leading to stronger absorption ability in the visible region, more red shifting, and a narrower band gap. Furthermore, with the increase of the doping nickel amount, the absorptions of all samples are strengthened in the visible region. It is generally accepted that the photocatalytic performance is determined by the light absorption ability, charge separation efficiency, and transfer rate to the surface of

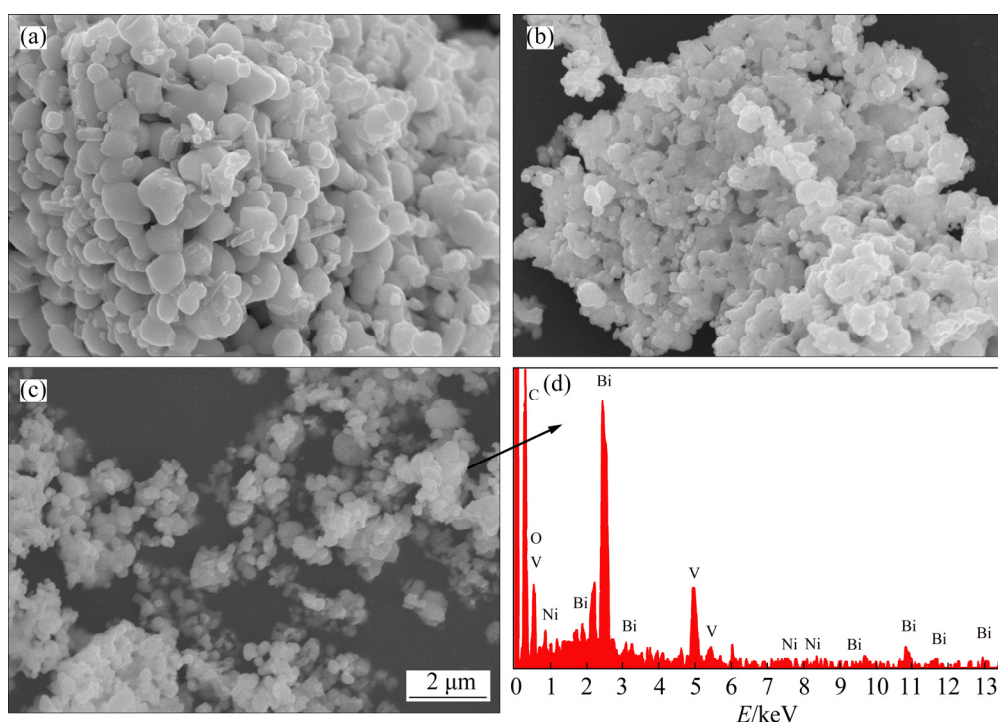


Fig. 3 SEM images of pure BiVO₄ (a), B–BiVO₄ (b), 0.30Ni–B–BiVO₄ (c) and EDX spectrum of 0.30Ni–B–BiVO₄ (d)

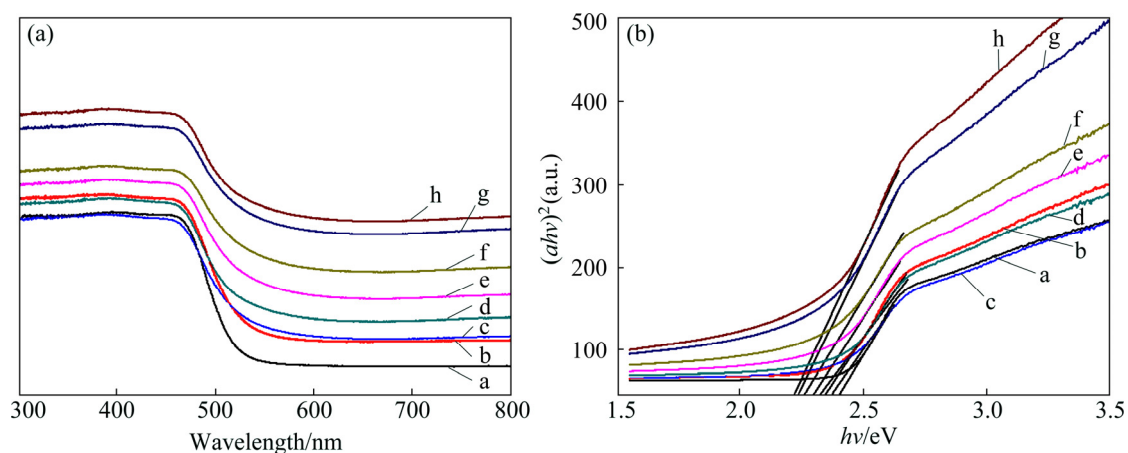


Fig. 4 UV–Vis absorption spectra (a) and $(ah\nu)^2-h\nu$ curves (b) of different samples: a—BiVO₄; b—B–BiVO₄; c—0.30Ni–BiVO₄; d—0.20Ni–B–BiVO₄; e—0.25Ni–B–BiVO₄; f—0.30Ni–B–BiVO₄; g—0.35Ni–B–BiVO₄; h—0.40Ni–B–BiVO₄

the photocatalysts. Consequently, the absorption ability of visible light for BiVO_4 is strengthened because nickel and boron co-doping can improve the photocatalytic activity. The Kubelka–Munk function, i.e., $ah\nu=c(h-E_g)^n$, was used to estimate the band gap energy of the as-prepared samples, where a is the absorption coefficient, $h\nu$ is the photon energy, c is a constant ($c=1$), E_g is the band gap energy, and n is a constant and is dependent on the type of semiconductor. In the case of BiVO_4 , n is equal to 0.5 and 2 for direct and indirect band gaps, respectively [17]. The results indicate that the band gap energies of BiVO_4 , B– BiVO_4 , 0.3Ni– BiVO_4 and $x\text{Ni-B-BiVO}_4$ ($x=0.20, 0.25, 0.30, 0.35, 0.40$) are 2.40, 2.36, 2.38, 2.33, 2.30, 2.26, 2.24 and 2.22, respectively.

3.4 Photocatalytic activity

The photocatalytic activities of BiVO_4 , B– BiVO_4 , Ni– BiVO_4 , and $x\text{Ni-B-BiVO}_4$ were evaluated by examining the degradation of MO. The change in MO concentration was determined by measuring the change of its characteristic absorption band at 452 nm. Figure 5(a) shows the degradation rate of MO over pure, B-doped, Ni-doped, and Ni–B co-doped BiVO_4 samples under visible light irradiation for 50 min. Figure 5(b) presents the kinetic curves for the photocatalytic degradation of MO, and the apparent rate constants of the samples were calculated according to the following formula: $\ln(c_0/c_t)=kt$, where c_0 and c_t are the initial and measured concentrations after irradiation for t min, respectively [21].

From Fig. 5(b), the reaction did follow a first-order mechanism, and the apparent rate constants obtained for different catalysts with different Ni contents are listed in Table 1. Furthermore, the results for the blank test demonstrate that the degradation of MO is slow without a photocatalyst. Compared with pure BiVO_4 , the MO photocatalytic degradation rate of the B-doped sample is higher. With Ni doping, the MO photocatalytic degradation rate of Ni–B co-doped BiVO_4 increases with Ni doping content up to 0.30%, but decreases when the amount of Ni is higher than 0.30%. The degradation rate of MO can reach 95% in 50 min, which shows that the optimal mass fraction of Ni doping is 0.30%.

The 0.3Ni–B– BiVO_4 was also used to photodegrade methyl blue (MB), acid orange II (AOII), rhodamine B (RhB) solutions. The changes in the absorption spectra of MB, AOII, RhB and MO solutions during the photodegradation process by 0.3Ni–B– BiVO_4 at different irradiation time are shown in Fig. 6. It was observed that the maximum absorption peaks of these four dye solutions decrease with increasing irradiation time. This indicated that the concentration of the dye solutions decreased in the presence of 0.3Ni–B– BiVO_4

and visible light illumination. So, we can conclude that the Ni–B co-doped BiVO_4 has a good photocatalytic activity for organic pollutants.

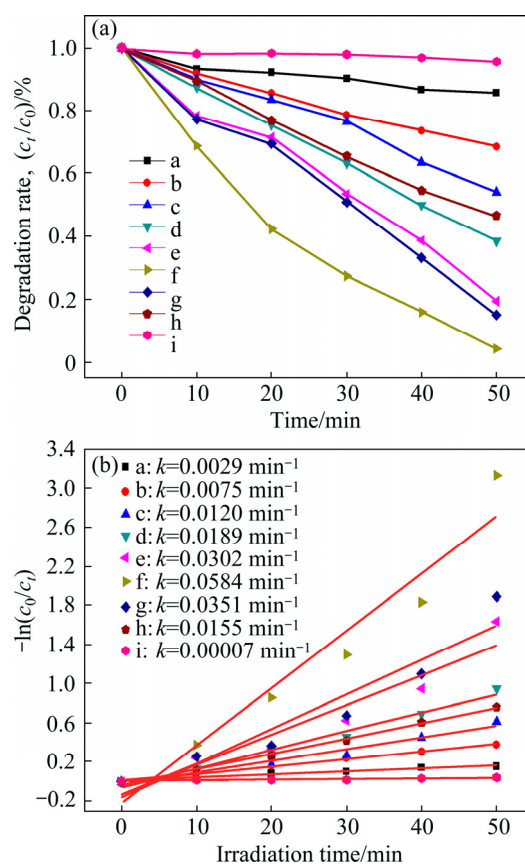


Fig. 5 MO degradation rate under visible light illumination for 50 min in the presence of B– BiVO_4 with various nickel doping, pure BiVO_4 and without photocatalyst (a), and $\ln(c_0/c_t)$ vs time curves of different samples (b): a— BiVO_4 ; b—B– BiVO_4 ; c—0.30Ni– BiVO_4 ; d—0.20Ni–B– BiVO_4 ; e—0.25Ni–B– BiVO_4 ; f—0.30Ni–B– BiVO_4 ; g—0.35Ni–B– BiVO_4 ; h—0.40Ni–B– BiVO_4 ; i—Blank

3.5 Mechanism for photocatalytic activity of Ni–B co-doped BiVO_4

In contrast with the undoped, B or Ni single doped BiVO_4 samples, the enhanced degradation of organic pollutants with the Ni–B co-doped sample under visible light irradiation can be explained as follows. Firstly, it is well known that the photoactivity of a catalyst is determined by the light absorption ability. The co-doped sample exhibits an enhanced visible light absorption property due to the B and Ni present in the substitutional positions in the BiVO_4 lattice. The dopants introduce more energy levels in the BiVO_4 band gap, thus leading to a narrower band gap in Ni–B– BiVO_4 catalysts. They improve the quantity of the photo-induced electrons and holes, and promote the photocatalytic rate. Secondly, the separation efficiency of photogenerated electrons and holes is an important factor determining the light

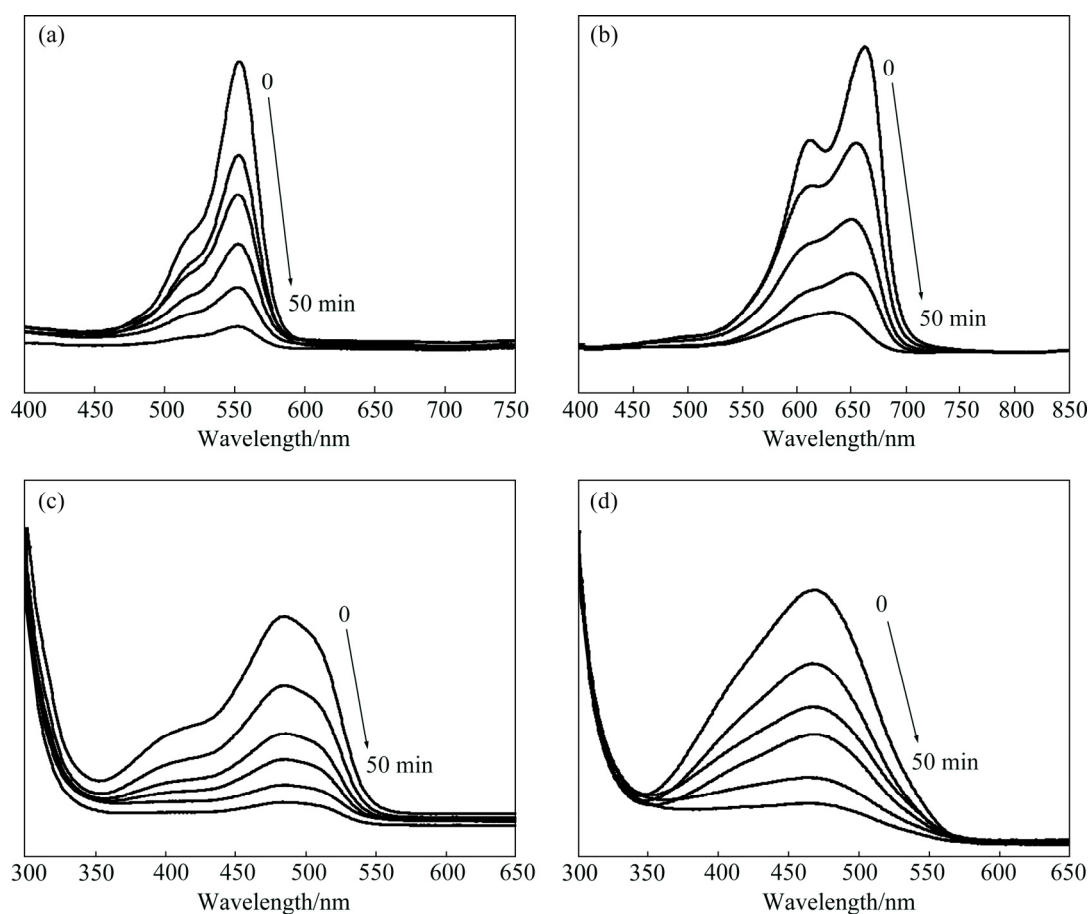


Fig. 6 UV-Vis absorption spectra of photocatalytic degradation of 10 mg/L RhB (a), 15 mg/L MB (b), 15 mg/L AOII (c) and 15 mg/L MO (d) by 0.3Ni-B-BiVO₄ samples at different irradiation time

quantum yield. The lower the recombination rate of the sample is, the higher the photoactivity is. The Ni-doping in B-BiVO₄ can effectively inhibit the recombination of photogenerated electrons and holes, thereby improving the quantum efficiency. Additionally, more V⁴⁺ ions, formed by Ni doping in B-BiVO₄, can also capture photo-induced electrons to form V⁵⁺, which is favorable for photocatalytic efficiency. Furthermore, the Ni-B co-doping further increases the concentration of surface hydroxyl oxygen (Oads) in BiVO₄ (as shown in Section 3.1), which is beneficial to photocatalytic process. The hydroxyl groups may accept photogenerated holes to produce strong oxidative hydroxyl free radicals (•OH) and H⁺ species. On the other hand, the surface hydroxyl groups can also act as adsorption centers for O₂ and organic molecules [30]. This reaction would occur via the following mechanism:

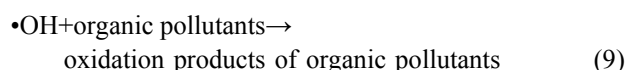
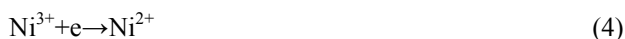


Photo-induced e/h⁺ pairs are generated on the surface of the photocatalyst during irradiation (Eq. (1)). The photo-induced electron (e) can be easily trapped by Ni³⁺ and V⁵⁺ ions (Eqs. (4) and (5)), thus effectively reducing the recombination of e/h⁺ pairs. The photo-induced h⁺ oxidizes H₂O molecules adsorbed on the photocatalyst surface into •OH and H⁺ species (Eq. (6)), while the photo-induced e can be captured by O₂ molecules adsorbed on the catalyst surface to form O₂⁻ species (Eq. (7)), and H⁺ reduces the active O₂⁻ species into •OH species (Eq. (8)). It is known that •OH species are the main active species in the photocatalytic reaction [29]. The organic molecules are oxidized by the •OH species into inorganic molecules (Eq. (9)). Therefore, we think that active V⁵⁺, Ni³⁺, and Oads species contribute to the direct or indirect generation of •OH species on the surface of the photocatalyst under visible light illumination, which promote the

photocatalytic degradation of MO. In other words, doping Ni^{2+} into the B– BiVO_4 lattice improves photocatalytic activity by increasing the concentrations of V^{4+} and Oads species.

In addition, it is generally accepted that photocatalytic performance is also influenced by the crystal structure, particle morphology and surface area [3,31]. In the present work, the samples had some similar physical properties such as monoclinic scheelite crystal structure and sphere-like particle morphology. The crystal structure and particle morphology are therefore not the main reasons for the higher photocatalytic activity of Ni–B co-doped BiVO_4 . However, as seen from the BET results, the surface areas of Ni–B co-doped BiVO_4 samples are larger than those of the undoped, B or Ni single doped BiVO_4 samples. We can therefore conclude that the increase in surface area by Ni–B co-doping may be another cause for the higher photocatalytic activity because photocatalytic reactions mainly take place on the photocatalyst's surface. The adsorption of target pollutants on the photocatalyst is also a key step in the photocatalytic reaction. Consequently, the stronger adsorption of organic pollutants and the improved microstructural properties both benefit to the enhanced photoactivity of the co-doped sample. In conclusion, all of the above factors resulting from Ni–B co-doping cause a synergetic effect to enhance the visible light activity.

However, Ni^{2+} ions can also act as recombination centers for the electrons and holes. Therefore, an adequate amount of doping Ni in the B– BiVO_4 catalysts is important so that the recombination of photogenerated electrons and holes can be suppressed effectively. As a consequence, the efficiency of the photocatalytic reaction is improved.

4 Conclusions

1) Ni-doped BiVO_4 samples with different Ni^{2+} doping concentrations were successfully prepared through sol–gel and impregnation two-step method. Compared with the undoped, B-, Ni-single doped BiVO_4 , the Ni–B co-doped BiVO_4 exhibits higher photoactivity under visible light, which shows higher photocatalytic performance for the MO degradation, and the highest degradation rate with 0.3Ni–B– BiVO_4 can reach approximately 96% under visible light irradiation for 50 min. The 0.3Ni–B– BiVO_4 sample can also effectively photodegrade RhB, MB and AOII.

2) All of the samples had single-phase monoclinic crystal structure and sphere-like particle morphology. Ni–B co-doped BiVO_4 leads to the narrower band gaps, the appearance of Ni^{2+} species and increased amounts of V^{4+} and Oads species. Moreover, Ni–B co-doping

increases the concentration of surface hydroxyls and the adsorption ability to organic substances.

3) The enhanced visible light activity for Ni–B co-doped BiVO_4 is ascribed to the synergetic effect of the increased visible light absorption ability, charge separation efficiency, surface hydroxyl and adsorption ability to organic pollutants.

References

- [1] HE Rong-an, CAO Shao-wen, ZHOU Peng, YU Jia-guo. Recent advances in visible light Bi-based photocatalysts [J]. Chinese Journal of Catalysis, 2014, 35(7): 989–1007.
- [2] CHEN Yuan, ZHOU Ke-chao, HUANG Su-ping, LI Zhi-you, LIU Guo-cong. Hydrothermal synthesis and photocatalytic property of BiVO_4 nanosheets [J]. The Chinese Journal of Nonferrous Metals, 2011, 21(7): 1570–1579. (in Chinese)
- [3] XU Lei, WEI Yong-ge, GUO Wan, GUO Yi-hang, GUO Ying-na. One-pot solvothermal preparation and enhanced photocatalytic activity of metallic silver and graphene co-doped BiVO_4 ternary systems [J]. Applied Surface Science, 2015, 332: 682–693.
- [4] ZHANG X F, DU L L, WANG H, DONG X L, ZHANG X X, MA C, MA H C. Highly ordered mesoporous BiVO_4 : Controllable ordering degree and super photocatalytic ability under visible light [J]. Microporous and Mesoporous Materials, 2013, 173: 175–180.
- [5] ZHOU Ying, LI Wei, WAN Wen-chao, ZHANG Rui-yang, LIN Yuan-hua. W/Mo co-doped BiVO_4 for photocatalytic treatment of polymer-containing wastewater in oilfield [J]. Superlattices and Microstructures, 2015, 82: 67–74.
- [6] SARKAR S, CHATTOPADHAYY K K. Visible light photocatalysis and electron emission from porous hollow spherical BiVO_4 nanostructures synthesized by a novel route [J]. Physica E: Low-dimensional Systems and Nanostructures, 2014, 58: 52–58.
- [7] OBREGÓN S, COLÓN G. Heterostructured Er^{3+} doped BiVO_4 with exceptional photocatalytic performance by cooperative electronic and luminescence sensitization mechanism [J]. Applied Catalysis B: Environmental, 2014, 158–159: 242–249.
- [8] ZHANG Bin, ZHAO Xu, LIU Hui-juan, QU Jiu-hui, HUANG C P. Synthesis of visible-light sensitive M– BiVO_4 (M=Ag, Co, and Ni) for the photocatalytic degradation of organic pollutants [J]. Separation and Purification Technology, 2011, 77: 275–282.
- [9] CHEN Yuan, YANG Jia-tian, PANG Qi, ZHOU Ke-chao, HUANG Jian-ying. Hydrothermal synthesis of visible light driven Ni– BiVO_4 photocatalysts and its photocatalytic performance [J]. Journal of Synthetic Crystals, 2013, 42: 1230–1236. (in Chinese)
- [10] ZHANG Jin, CUI Hao, WANG Bing, LI Chuang, ZHAI Jian-ping, LI Qin. Preparation and characterization of fly ash cenospheres supported CuO– BiVO_4 heterojunction composite [J]. Applied Surface Science, 2014, 300: 51–57.
- [11] GAO Xiao-ming, FU Feng, ZHANG Li-ping, LI Wen-hong. The preparation of Ag– BiVO_4 metal composite oxides and its application in efficient photocatalytic oxidative thiophene [J]. Physica B: Condensed Matter, 2013, 419: 80–85.
- [12] CHALA S, WETCHAKUN K, PHANICHPHANT S, INCEESUNGVORN B, WETCHANUM N. Enhanced visible-light-response photocatalytic degradation of methylene blue on Fe-loaded BiVO_4 photocatalyst [J]. Journal of Alloys and Compounds, 2014, 597: 129–135.
- [13] LUO Yang-yang, TAN Guo-qiang, DONG Guo-hua, ZHANG Li-li, HUANG Jing, YANG Wei, ZHAO Cheng-cheng, REN Hui-jun. Structural transformation of Sm^{3+} doped BiVO_4 with high photocatalytic activity under simulated sun-light [J]. Applied Surface

- Science, 2015, 324: 505–511.
- [14] ZHANG Yao-hong, YI Zhi-guo, WU Guo-hua, SHEN Qing. Novel Y doped BiVO₄ thin film electrodes for enhanced photoelectric and photocatalytic performance [J]. Journal of Photochemistry and Photobiology A: Chemistry, 2016, 327: 25–32.
- [15] LUO Yang-yang, TAN Guo-qiang, DONG Guo-hua, REN Hui-jun, XIA Ao. A comprehensive investigation of tetragonal Gd-doped BiVO₄ with enhanced photocatalytic performance under sun-light [J]. Applied Surface Science, 2016, 364: 156–165.
- [16] JIANG Hai-yan, DAI Hong-xin, DENG Ji-guan, LIU Yu-xi, ZHANG Lei, JI Ke-meng. Porous F-doped BiVO₄: Synthesis and enhanced photocatalytic performance for the degradation of phenol under visible-light illumination [J]. Solid State Sciences, 2013, 17: 21–27.
- [17] ZHAO Zhen-xuan, DAI Hong-xing, DENG Ji-guang, LIU Yu-xi, AU C K. Effect of sulfur doping on the photocatalytic performance of BiVO₄ under visible light illumination [J]. Chinese Journal of Catalysis, 2013, 34(8): 1617–1626.
- [18] WANG Min, LIU Qiong, CHE Yin-sheng, ZHANG Li-fang, ZHANG Dong. Characterization and photocatalytic properties of N-doped BiVO₄ synthesized via a sol-gel method [J]. Journal of Alloys and Compounds, 2013, 548: 70–76.
- [19] TAN Guo-qiang, ZHANG Li-li, REN Hui-jun, HUANG Jing, YANG Wei, XIA Ao. Microwave hydrothermal synthesis of N-doped BiVO₄ nanoplates with exposed (040) facets and enhanced visible-light photocatalytic properties[J]. Ceramics International A, 2014, 40: 9541–9547.
- [20] WANG Min, ZHENG Hao-yan, LIU Qiong, NIU Chao, CHE Yin-sheng, DANG Ming-yan. High performance B-doped BiVO₄ photocatalyst with visible light response by citric acid complex method [J]. Spectrochimica Acta A: Molecular and Biomolecular Spectroscopy, 2013, 114: 74–79.
- [21] WANG Min, NIU Chao, LIU Jun, WANG Qian-wu, YANG Chang-xiu, ZHENG Hao-yan. Enhanced visible-light-driven photocatalytic activity of B-doped BiVO₄ synthesized using a corn stem template [J]. Materials Science in Semiconductor Processing, 2015, 30: 307–313.
- [22] LI Yan-qing, JING Tao, LIU Yuan-yuan, HUANG Bai-biao, DAI Ying-dai, ZHANG Xiao-yang, QIN Xiao-yan, WHANGBO M H. Enhancing the efficiency of water oxidation by boron-doped BiVO₄ under visible light: Hole trapping by BO₄ tetrahedra [J]. Chem Plus Chem, 2015, 80: 1113–1118.
- [23] ZHOU Yi, HUANG Ke-long, ZHU Zhi-ping, XIA Chang-bin. Eu²⁺/Gd³⁺-codoped nanocrystalline titania catalyst and its photocatalytic activity under natural light [J]. Transactions of Nonferrous Metals Society of China, 2007, 17(S3): s1112–s1116.
- [24] PATEL N, JAISWAL R, WARANG T, SCARDUELLI G, DASHORA A, AHUJA B L, KOTHARI D C, MIOTELLO A. Efficient photocatalytic degradation of organic water pollutants using V–N co-doped TiO₂ thin films [J]. Applied Catalysis B: Environmental, 2014, 150–151: 74–81.
- [25] KIMA T H, RODRÍGUEZ-GONZÁLEZ V, GYAWALI G, CHO S H, SEKINO T, LEE S W. Synthesis of solar light responsive Fe, N co-doped TiO₂ photocatalyst by sonochemical method [J]. Catalysis Today, 2013, 212: 75–80.
- [26] WANG Min, CHE Yin-sheng, NIU Chao, DANG Min-yan, ZHANG Dong. Effective visible light-active boron and europium co-doped BiVO₄ synthesized by sol-gel method for photodegradation of methyl orange [J]. Journal of Hazardous Materials, 2013, 262: 447–455.
- [27] WANG Min, CHE Yin-sheng, NIU Chao, DANG Min-yan, ZHANG Dong. Lanthanum and boron co-doped BiVO₄ with enhanced visible light photocatalytic activity for degradation of methyl orange [J]. Journal of Rare Earths, 2013, 31: 878–884.
- [28] LONG Hui-jin, MENG Qing-ju, YUAN Jin, YANG Wen-sheng, CAO Ya-an. Study on photocatalytic activity of boron doped TiO₂ catalyst [J]. Acta Chimica Sinica, 2008, 66: 657–661. (in Chinese)
- [29] WEI Feng-yu, NI Liang-suoi. Photocatalytic performance and doping mechanism of B–S co-doped TiO₂ [J]. Chinese Journal of Catalysis, 2007, 28: 905–909.
- [30] UMAPATHY V, MANIKANDAN A, ARUL ANTONY S, RAMU P, NEERAJA P. Structure, morphology and opto-magnetic properties of Bi₂MoO₆ nano-photocatalyst synthesized by sol-gel method [J]. Transactions of Nonferrous Metal of China, 2015, 25: 3271–3278.
- [31] JIANG Hai-yan, DAI Hong-xin, MENG Xue, ZHANG Lei, DENG Ji-guang, JI Ke-meng. Morphology dependent photocatalytic performance of monoclinic BiVO₄ for methyl orange degradation under visible-light irradiation [J]. Chinese Journal of Catalysis, 2011, 32: 939–949.

Ni 掺杂量对溶胶-凝胶和浸渍两步法制备 B-BiVO₄ 光催化活性的影响

王 敏, 杨光俊, 由美雁, 谢元华, 王有昭, 韩 进, 朱 彤

东北大学 机械工程与自动化学院, 沈阳 110165

摘 要: 为了进一步提高 B-BiVO₄ 的光催化活性, 通过溶胶-凝胶和浸渍两步法制备 Ni 掺杂 B-BiVO₄ 光催化剂 (Ni-B-BiVO₄)。通过 XPS、XRD、SEM、BET、EDS 和 UV-Vis 等手段对样品进行表征。结果表明, 单或共掺杂均不会改变样品的晶型和形貌; 但当掺入 Ni 后, 样品的晶体粒径减小。与未掺杂、B 以及 Ni 单掺杂相比, Ni-B-BiVO₄ 样品的光吸收向长波长方向偏移; 且 N-B 共掺杂后, 样品中 V⁴⁺ 和表面羟基氧增多。当最佳 Ni 掺杂量为 0.30%(质量分数)时, 所制备的 0.3Ni-B-BiVO₄ 在 50 min 内对甲基橙的降解率达 95%左右, 且该样品能有效降解亚甲基蓝(MB)、金橙 II 号(AOII)和罗丹明 B(RhB)溶液。共掺杂样品活性的提高主要是 B 与 Ni 的协同作用所致。

关键词: 共掺杂; 镍掺杂; BiVO₄; 光催化剂; 溶胶-凝胶法; 浸渍法

(Edited by Wei-ping CHEN)